Article:
Bell, AJ orcid.org/0000-0002-2061-3862, Shepley, PM orcid.org/0000-0003-1240-593X and Li, Y (2020) Domain Wall Contributions to Piezoelectricity in Relaxor-Lead Titanate Single Crystals. Acta Materialia, 195. pp. 292-303. ISSN 1359-6454

https://doi.org/10.1016/j.actamat.2020.05.034

Domain Wall Contributions to Piezoelectricity in Relaxor-Lead Titanate Single Crystals

Andrew J. Bell*, Philippa M. Shepley and Yang Li

School of Chemical and Process Engineering, University of Leeds,

Woodhouse Lane, Leeds, LS2 9JT, UK

*Corresponding author: E-mail - a.j.bell@leeds.ac.uk; Phone - +44 1133 432370

Keywords: ferroelectricity, piezoelectricity, relaxor

Abstract

It is demonstrated that the dielectric permittivity and piezoelectric coefficients in relaxor-$PbTiO_3$ single crystals close to the morphotropic phase boundary (MPB) can be augmented by contributions from domain walls. Landau-Ginzburg-Devonshire models, incorporating both polarization and strain gradients through the domain walls, show that wall contributions in domain engineered single crystals originate from enhanced, field-induced polarization rotation in static domain walls, unlike ceramics, in which piezoelectricity is enhanced by domain wall translation. For 71° domain walls in 0.7 $Pb(Mg_{1/3}Nb_{2/3})O_3 – 0.3PbTiO_3$ the piezoelectric charge coefficient d_{33} at the center of the wall ranges from 5000 to >30,000 pC N^{-1} depending on the wall width. Thus, a sufficiently high domain wall density can account for the experimentally observed augmentation in the measured properties compared to single domain models. The symmetry of the domain walls explains both the variety of average symmetries observed close to the MPB and the experimentally observed switching of the $[001]$-oriented crystals into the tetragonal phase via a symmetry-improbable M_C phase. For a crystal of rhombohedral ground state, the presence of domain walls will impart monoclinic symmetry, the predominance of which increases with increasing domain wall density.

1. Introduction

Single crystals of lead-based relaxors in solid solution with lead titanate, such as $Pb(Mg_{1/3}Nb_{2/3})O_3$-$PbTiO_3$ (PMN-PT), are the highest performing of known piezoelectric materials in terms of their piezoelectric coupling coefficient (k_{33} ≈ 0.9) and piezoelectric charge coefficient (d_{33} > 2000 pC N^{-1}). [1, 2] These values correspond to approximately three times the charge coefficient of commercial ceramic Pb(Zr, Ti)O_3 (PZT) and with 60% greater energy conversion. They are the preferred materials for the manufacture of ultrasound imaging transducers [3] and sonar devices [4], as well as finding new applications in high power electromechanical devices. [5] Whilst their room temperature piezoelectric performance is unique amongst piezoelectric materials, the disadvantageously low Curie temperature (T_C = 130 to 180°C) and the imperative to eradicate lead in electronic materials [6] is driving a search for new, particularly lead-free, materials, but with improved properties compared to the present generation of single crystals. It is therefore important that we fully understand the origin of the "giant" piezoelectric properties in this class of materials.

Since the first demonstration of the large piezoelectric activity in these crystals, [1] the most commonly cited mechanism has been polarization rotation. The highest performing crystals have compositions close to what is known as a morphotropic phase boundary (MPB), a boundary separating two perovskite symmetries in the composition-temperature phase diagram. The boundary is also apparent in the corresponding phase diagrams for the variables of electric field and stress. In the case of PMN-PT, the phase sequence on passing through the boundary can be complex and is dependent not only on composition and sample history, but also it is particularly sensitive to the direction and magnitude of the poling and measurement fields. Here, we initially describe the conventional polarization rotation model in terms of a simplified phase boundary

between the rhombohedral $R3c$ symmetry and the tetragonal $P4mm$, with fields applied parallel to the *[001]* direction. An unpoled crystal on the PMN-rich, rhombohedral side of the boundary comprises eight domain variants with polar axes parallel to the $\langle 111 \rangle$ directions. Following the temporary application of a sufficiently large, positive, poling field parallel to the *[001]* direction, only the 4 domain variants with a positive l Miller index remain, resulting in an average macroscopic polar direction parallel to *[001]* (Fig. 1(a)). Subsequent *[001]* field excursions result in large piezoelectric distortion due to the polar axis in each domain rotating towards the *[001]* direction via a monoclinic symmetry that is intermediate to the tetragonal and rhombohedral forms. This model is informed by X-ray diffraction under applied field [7], confirming that the average symmetry under increasing applied fields transforms from approximately rhombohedral, through a monoclinic phase to the tetragonal. There are alternative monoclinic symmetries governing the path the polarization rotation takes. These differ in the orientation of the plane within which the polarization lies and are often designated M_A, M_B and M_C; as shown in Fig. 1(b). In the M_A and M_B phases, the polarization vector lies within a *{110}* plane, whilst the polarization vector of the M_C phase lies within a {100} plane. According to Baia et al. [7] for 0.7 $Pb(Mg_{1/3}Nb_{2/3})O_3$-0.3 $PbTiO_3$, on *[001]*-poling, the average zero-field symmetry changes from rhombohedral to M_A. However, as the angle between the M_A polar direction and $\langle 111 \rangle_{+l}$ is very small, a model with $R3c$ as the zero-field state is still conceptually valid. It was also shown [7] that on applying an increasing electric field to a *[001]*-poled crystal, that whilst the symmetry at low field is M_A, with polarization rotating in the *{110}* planes, it switches to M_C, with the polarization completing its rotation towards *[001]* in the *[100]* or *[010]* planes. Considering the symmetry of the initial and final states, combined with the

direction of the applied field, switching via the M_C phase is counterintuitive compared to a continuous M_A path.

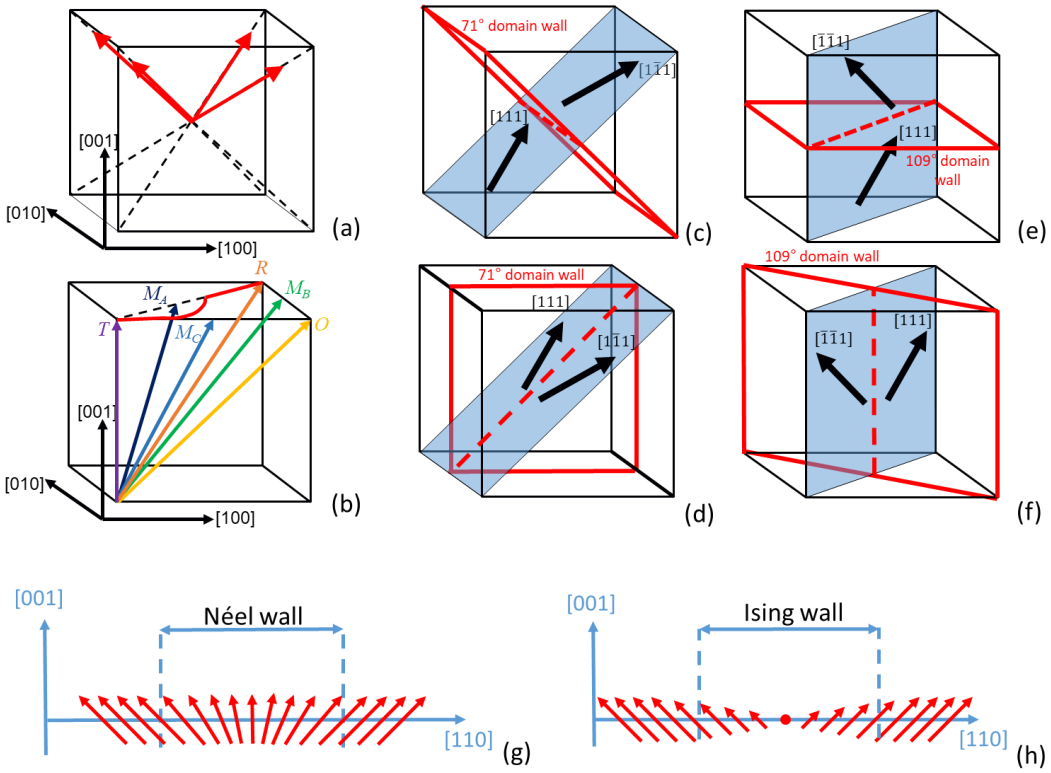

Figure 1. (a) Orientation of polarization vectors (red arrows) in the domain variants in a *[001]*-poled rhombohedral crystal and (b) example polarization vectors corresponding to monoclinic symmetry (M_A, M_B and M_C), compared to tetragonal (T), orthorhombic (O) and rhombohedral (R) in perovskite crystals; the experimentally observed high-field polarization rotation path in PMN-PT[7] is marked in red; (c) and (d) example polarization orientations for 71° and (e) and (f) 109° domain walls in a *[001]*-poled rhombohedral perovskite crystal; schematic of polarization vectors in (g) Néel and (h) Ising model domain walls.

In addition to the MPB, a common feature of single crystals with giant piezoelectric activity is that their non-$PbTiO_3$ end members are classified as relaxors, the properties of which are widely attributed to the dynamics of microscopic fluctuations of the polarization, so-called polar nanoregions (PNRs). [8] The relaxor phenomenon originates in the of chemical disorder in the crystal lattice giving rise to random, local electric fields or lattice strains [9] that limit the polar coherence length resulting in the existence of PNRs rather than long-range, coherent polarization. In the case of PMN-PT, although the addition of PT increases chemical disorder, it also increases the polar

coherence length in the solid solution, such that compositions beyond 0.6PMN-0.4PT are not relaxors, but true ferroelectrics. This relaxor-ferroelectric boundary is also close to the MPB, hence the key compositions close to 0.7PMN-0.3PT, whilst exhibiting some relaxor characteristics around the peak in permittivity close to T_C, effectively behave as ferroelectrics at room temperature, exhibiting aspects of conventional long-range ferroelectric order, including the presence of macroscopic ferroelectric and ferroelastic domains.

A key question in developing improved materials is whether it is the proximity to the MPB or the chemical disorder that is more dominant in developing giant piezoelectricity. Such discussions are hindered by the rarity of MPB single crystals in which a relaxor phase is not an end member. Hence, it is difficult to test the hypothesis that the phenomenon is mainly due to MPB-enhanced polarization rotation.

Although the polarization rotation model recognizes the existence of multiple domain states within the poled crystals, polarization rotation is often described as a purely macroscopic phenomenon occurring within a single domain state and does not introduce any aspects of domain wall dynamics. As we demonstrate below, such a macroscopic model is consistent with Landau-Devonshire theory [10] over a wide temperature range. However, this model breaks down at low temperatures ($\lesssim$ 100 K) where a major relaxation of the dielectric permittivity is observed experimentally.[11] The relaxation in permittivity is also observed in the piezoelectric charge coefficients [12] and as the charge coefficient and permittivity are closely related, it can be assumed that the two relaxations are of the same origin. Circumstantially, there is an implication that the polarization mechanism that relaxes below 100 K is also responsible for the giant room temperature piezoelectricity in *[001]*-oriented crystals; the nature of the relaxation suggests that the mechanism is temperature activated. However,

macroscopic polarization rotation, as described above, is free of temperature-activated phenomena; there is no activation energy in the rotation model. Such behavior begs the question of whether a more microscopically based model should be considered.

Recently the potential role of cation disorder has been highlighted by Li et al., [12, 13] who have developed a 2-dimensional phase-field model for the case of a tetragonal single crystal in which the cation disorder produces localized orthorhombic regions. These result in an augmentation of the piezoelectric coefficient and relative permittivity due to field-stabilization (rotation) of the orthorhombic polarization towards the *[001]* direction. The origin of the relaxation at 100 K is shown to be freezing-in of the orthorhombic state. It is inferred that for the real case of PMN-PT, a 3D model of tetragonal fluctuations in a rhombohedral matrix would apply.

Nevertheless, the above model is difficult to reconcile with recent experimental data. Shepley et al. [14] have characterized single crystals of $Pb(In_{1/2}Nb_{1/2})O_3$-$Pb(Mg_{1/3}Nb_{2/3})O_3$-$PbTiO_3$ before and after poling in the *[001]* and *[111]* directions. The composition is rhombohedral, but is close to the MPB with the tetragonal phase and exhibits similar properties to 0.7PMN-0.3PT, but with a slightly higher Curie temperature. Before poling, the permittivity appears to be virtually identical for the *[001]* and *[111]* directions. However, after poling, the *[001]*-oriented crystal exhibits a significant increase in permittivity at room temperature, with a major relaxation below 100K, whilst the permittivity of the *[111]*-oriented crystal decreases markedly on poling, with only a small relaxation around 100 K. It is not clear how the phase fluctuation model would account for such distinctive behavior.

Moreover, it has been shown for 0.7 PMN-0.3PT crystals that AC poling regimes result in both an increase in the domain wall density and an enhancement of the permittivity and piezoelectric charge coefficient compared to conventional DC poling.

[15] Similarly, Yu et al. [16] showed an increase in the d_{33} of $Pb(Zn_{1/3}Nb_{2/3})O_3$ - $PbTiO_3$ with increased nucleation of domains due to pulse poling. PMN-PT has been recognized as a "domain boundary-dominated system", [17] one in which the density of domain walls is exceptionally high and in which specific conformations of high symmetry domains can lead to lowering of the average macroscopic symmetry [18].

In conventional ferroelectric crystals, Akishige et al measured a large dielectric relaxation around 100K in top-seeded solution grown $BaTiO_3$ single crystals,[19] whilst Wada et al. [20] have also shown that increasing domain wall density in $BaTiO_3$ single crystals results in an increase in the piezoelectric charge coefficient. In all the above cases the orientation of the field with respect to the crystal prohibits ferroelastic domain wall motion, thought to be responsible for significant contributions to piezoelectricity in PZT ceramics. However, Rao and Wang [21] have proposed a domain wall broadening mechanism to account for the results of Wada, [20] which suggests that broadening of non-Ising walls is responsible for increases in piezoelectric activity in domain engineered crystals such as $BaTiO_3$ and PMN-PT.

In this paper we investigate the potential role of domain walls in facilitating polarization rotation in PMN-PT type single crystals at both low and high fields and as a function of composition near the MPB, through a one-dimensional Landau-Ginzburg Devonshire (LGD) model of the polar structure of 71° and 109° domain walls.

2. Theory

In the following, we assume a rhombohedral ground state for the infinite domain-free crystal. Although this may appear to contradict experimental evidence for the crystals studied, one of the objectives of this work is to demonstrate that rhombohedral crystals

with high domain wall densities will exhibit an average, monoclinic symmetry to a probe of sufficiently long coherence length (e.g. X-rays).

Throughout the following discussion, the polarization vector is treated as the resultant of three orthogonal vectors parallel to the *<100>* directions of the crystal. In a *[001]*-poled rhombohedral crystal, there are generally four types of domain walls, as shown in Fig. 1(c-f). In all cases, the domain walls separate polarization vectors that lie in the same *{110}* plane and correspond to mirror planes between the two polar axes. In two cases, the polarization directions lie approximately 71° apart, with only one of the orthogonal components of polarization changing sign through the wall (Figs. 1(c) & (d)), whilst for the two 109° walls, two components change sign (Figs. 1(e) & (f)). Conventionally, there is a further distinction between the domain types depending on whether the component of polarization normal to the domain wall changes sign or not. In the former case, (Figs. 1(d) & (f)) such domain walls are regarded as being charged, whereas for those in which the normal component does not change sign (Figs. 1(c) & (e)), the domain wall is said to be uncharged. Conventional wisdom suggests that so-called charged domain walls are rare. However, if, as shown below, the change of sign is accomplished over a significant number of unit cells, the electrostatic hindrance to charged walls may be less than is intuitively expected.

Assuming the domain walls to be larger than one unit-cell in width, the change in magnitude and direction of polarization on passing through a wall may, in principle, correspond to Bloch, Néel (Figs 1(g)) or Ising (Fig. 1(h)) configurations. Bloch walls comprise rotation of the polarization vector out of the common *{110}* plane and are therefore considered unlikely close to an MPB which favors *<111>* and *<100>* orientations. In both Néel and Ising configurations, the polarization vector remains within the common *{110}* plane. For Ising walls, the magnitude of polarization decreases

towards the center of the wall, with the change of direction occurring only at the wall center, whilst for Néel walls the direction of polarization rotates through the wall, whilst the magnitude remains approximately constant. In the case of Néel walls, assuming a gradual rotation of the polarization vector between the two domain orientations, the orientation of the polarization at the center of a 71° domain wall is parallel to a $[101]$ direction, corresponding to orthorhombic symmetry, but with the outer parts of the wall exhibiting M_B symmetry. For a 109° wall, the polarization at the center would be parallel to $[001]$, corresponding to tetragonal symmetry, with the remainder of the wall being M_A. Hence, under $[001]$ applied fields a Néel wall could act as a nucleation site for initiation of polarization rotation. Also, for a crystal with a homogenous rhombohedral ground state, but with a high density of Néel walls, the average symmetry may depart from rhombohedral towards M_A or M_B.

The Landau-Devonshire model for ferroelectrics considers the free energy density due to the ferroelectric state, G, to be a power series expansion in terms of polarization. [10] In the stress-free case,

$$G(\boldsymbol{P}) = \alpha_{mnp}P_i^2 + \alpha_{mnp}P_i^2P_j^2 + \alpha_{mnp}P_i^2P_j^2P_k^2 - E_iP_i, \quad (1)$$

in which P_i are the components of the polarization vector $\boldsymbol{P}$. Likewise, $\boldsymbol{E}$ is the applied electric field. The coefficients α_{mnp}, hereafter known as the Landau coefficients, are the non-linear dielectric stiffness coefficients for the 2nd, 4th and 6th power of polarization; the subscripts take the values of the powers of the three components of polarization. Only the first order dielectric stiffness is required to be temperature dependent and is of the form $\alpha_{200} = \alpha'(T\text{-}T_0)$, where T is temperature and T_0 is the Curie-Weiss temperature. The spontaneous strains associated with the polarization in the absence of applied stress can be calculated from

$$x_{ij} = Q_{ijkl}P_kP_l, \quad (2)$$

where Q_{ijkl} are the electrostriction coefficients.

In the case of spatially non-uniform polarization, Ginzburg [22] proposed a simple method of incorporating polarization gradients into the theory, avoiding full solutions to the Maxwell equations, by including energy terms dependent upon the polarization gradient, of the form

$$|\alpha_{200}|\gamma_{ij}^2\left(\frac{dP_i}{dr_j}\right)^2, \tag{3}$$

in which γ_{ij} is the polarization coherence length and $\frac{dP_i}{dr_j}$ is the gradient of P_i in direction j. The gradient in polarization through a domain wall will also result in a gradient in strain, which can give rise to stress components within the wall. In this case it is more appropriate to use the H

$$F(\boldsymbol{P},\boldsymbol{x}) = \alpha'_{mnp}P_i^2 + \alpha'_{mnp}P_i^2P_j^2 + \alpha'_{mnp}P_i^2P_j^2P_k^2 - E_iP_i$$

$$+\frac{1}{2}c_{ijkl}x_{ij}x_{kl} - q_{ijkl}x_{ij}P_kP_l + |\alpha_{200}{}'|\gamma_{ij}^2\left(\frac{dP_i}{dr_j}\right)^2 + c_{ijkl}\delta_{ij}^2\left(\frac{dx_{ij}}{dr_j}\right)^2, \tag{4}$$

In the following, the equilibrium values of $\boldsymbol{P}$ and $\boldsymbol{x}$ are determined by numerical minimization of F with respect to $\boldsymbol{P}$ and $\boldsymbol{x}$ for given values of $\boldsymbol{E}$ and T. Permittivity is determined numerically from $\varepsilon_{ij} = \frac{\Delta P_i}{\Delta E_j}$ and the piezoelectric charge coefficient ($\boldsymbol{d}$) is calculated from $d_{ijk} = \frac{\Delta x_{ij}}{\Delta E_k}$, where ΔE is a small probe field of magnitude 1 kV m^{-1}. By convention, the component P_3 is parallel to the *[001]* direction.

To check for self-consistency, values of polarization for the homogenous, stress-free case were determined by minimisation of G with respect to $\boldsymbol{P}$ (Eqn. (1)) and the strains calculated from the electrostriction equation (Eqn. (2)); the results were identical to the polarizations and strains found by minimization of F with respect to $\boldsymbol{P}$ and $\boldsymbol{x}$ with no gradients in the order parameters.

To determine the influence of electric field upon domain walls, we have constructed simple one-dimensional finite element models of 71° and 109° domain walls in a *[001]*-poled PMN-PT crystal, based on the Helmholtz potential in Eqn. (4). The model comprises 100 cells, each of which is seeded with a value of spontaneous polarization resulting from the solution for the stress-free homogeneous system. To allow a one-dimensional model to represent a 3D system, it is assumed that γ_{ij} is isotropic (referred to hereon as γ), and all 3 polarization components couple from cell to cell. The only strain gradients which can influence the solutions are those for which there is cell to cell strain coupling along the direction normal to the domain wall. The details of the models are shown in Table 1.

For the 71° walls, cells 1 to 50 are seeded with solutions for the homogeneous system ($\gamma = \delta = 0$) which are initially constrained to $P_1 = -P_2 = P_3$, whilst for cells 51 to 100 initial solutions are constrained to $P_1 = P_2 = P_3$ with P_3 positive. This results in a domain wall of zero width at the interface between cells 50 and 51. For 109° walls, the corresponding initial constraints are $-P_1 = -P_2 = P_3$ and $P_1 = P_2 = P_3$. The structure of the domain wall is then allowed to evolve by minimization of $F(\boldsymbol{P}, \boldsymbol{x})$ for each cell, including the gradient terms, and then iterating until the total polarization and free energy for the array converge. The polarization gradient terms for the n^{th} cell are introduced as:

$$\left(\frac{dP_i}{dr}\right)^2 = \left(\left(P_i(n) - P_i(n-1)\right)^2 + \left(P_i(n) - P_i(n+1)\right)^2\right)/2, \quad (2)$$

where $P_i(n)$ is the subject of the current iteration and $P_i(n-1)$ and $P_i(n+1)$ are values from the previous iteration. A similar procedure is followed for strain gradients. As r, γ and δ share the same dimensions, the length scale is effectively dimensionless. The above methodology provides the freedom for Ising, Néel or Bloch wall structures to

develop from the convergence process. The total polarization and free energy of the arrays converge to better than 1 in 10^7 and 1 in 10^8 respectively, within 500 to 5000 iterations, depending on the magnitudes of γ, δ and applied electric field. As each energy minimization step employs the previous step's values of polarization and strain as a starting point and the methodology does not seek minima far from the previous iteration, phemomena such as domain wall splitting may be missed by the method.

The stress distributions in the wall were calculated by solving

$$x_{ij} = s_{ijkl}X_{kl} + Q_{ijlk}P_kP_l \quad (3)$$

for X_{kl} as a function of position, n. The contribution of the domain wall to the weak field permittivity, $\Delta\varepsilon_{33}$, is estimated by calculating the difference in the average polarization

$$\overline{P_3} = (\sum_n P_3(n))/N \quad (4)$$

for E_3 = 0 and E_3 = 1000 V m^{-1} and then subtracting the homogeneous contribution, where N is the total number of cells.

The piezoelectric coefficient of each cell is calculated from

$$d_{3i} = \Delta x_{ii}/E_3 \quad (5)$$

where Δx_{ii} is the change in strain on application of field for applied fields of E_3 = 0 and E_3 = 1000 V m^{-1}. The electrostriction coefficients, Q_{11} and Q_{12} are assumed to be independent of temperature. The charge coefficient for the whole array is taken as the average of the individual cell contributions.

The Landau coefficients in Eqns. (1) and (4) are those presented by Zhang et al for PMN-0.3PT.[27] Zhang's method of determination of the Landau coefficients is based on high field measurement and therefore they are free of domain wall contributions.

3. Results

3.1 Single Domain Polarization Rotation

Initially we consider the homogeneous model ($\gamma = \delta = 0$) for an infinite single domain of 0.7PMN-0.3PT. Fig. 2(a) shows the *(110)* free energy surface $G(\boldsymbol{P})$ at 300 K, with local minima in directions corresponding to *<001>*, *<011>* and *<111>*. Fig. 2(b) plots the locus of minimum G, as a function of the angle θ, between the resultant polarization and the *[001]* direction. The absolute minima lie at ±54.7° and ±125.3°, corresponding to the *<111>* directions and representing rhombohedral symmetry; the secondary minima at 0° and 180° are metastable tetragonal states. The apparent maxima at ±90° correspond to orthorhombic symmetry; we note that these are saddle points on the free energy surface and so still represent relatively low-lying energy states on the surface depicted in Fig. 2(a).

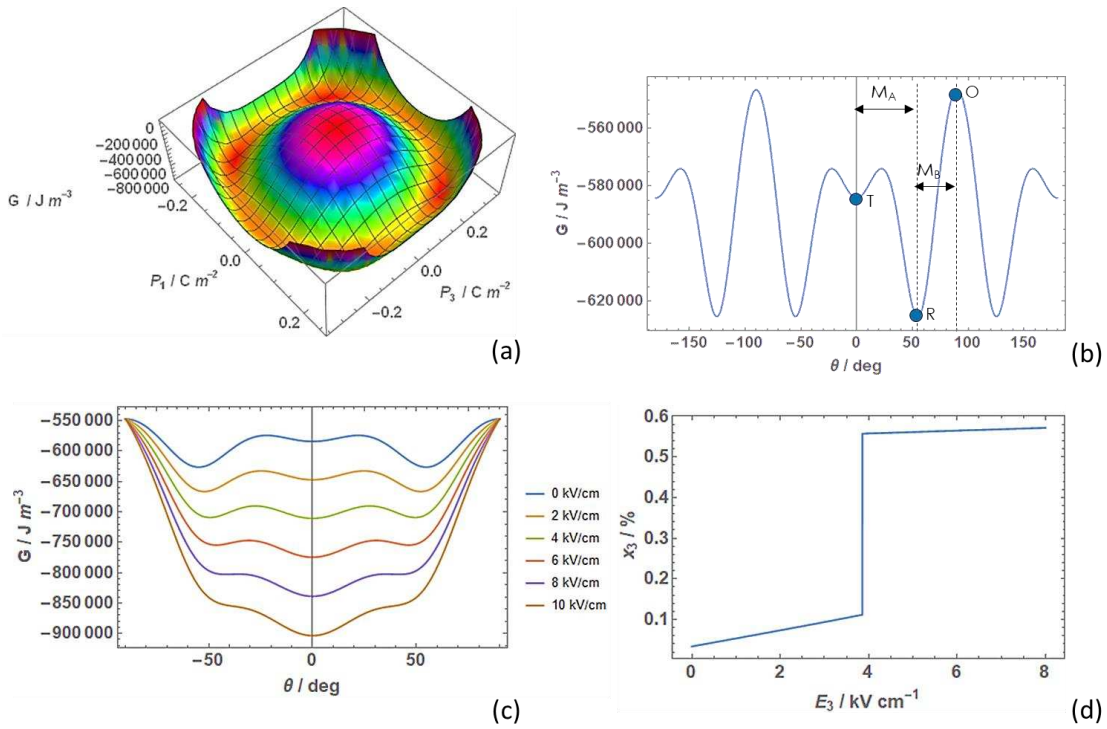

Figure 2. (a) Free energy surface in the *(110)* plane for 0.7PMN-0.3PT as a function of polarization with $P_1 = P_2$, (b) free energy density as a function of the angle of the resultant polarization, θ, to the *[001]* axis, (c) free energy as function of θ and applied field, E_3 and (d) lattice strain parallel to *[001]* as a function of applied field E_3.

Fig. 2(c) shows $G(\theta)$ as a function of applied field E_3. At low applied field, the minimum energy moves to decreasing values of θ, corresponding to M_A symmetry. At a

critical field value of 4 kV cm^{-1}, the minimum energy state shifts discontinuously to θ = 0°corresponding to a first order transition to tetragonal symmetry. This is confirmed by the discontinuity in lattice strain (x_3) as a function of field, as shown in Fig.2(d). The continued existence of the metastable M_A state above 4 kV cm^{-1} indicates that the field induced transition would exhibit hysteresis and that at low temperatures the transition may appear temperature activated. However, there is no activation energy involved in the weak field polarization rotation in the *(110)* plane and attendant properties, so this would not explain the experimentally observed 100 K relaxation in weak field properties. There is no value of field where a monoclinic M_C phase is the most stable; indeed, the symmetry of a field applied parallel to *[001]* in a rhombohedral or M_A crystal renders an M_C solution highly improbable, hence the experimental observation of a field-induced M_C phase [7] requires an additional mechanism to that of the homogeneous LGD crystal.

3.2 Domain Wall Structure

For brevity, we have assumed the most likely scenario, in which the polarization and strain coherence lengths are equal. Hence simulations were carried out for $\gamma = \delta$ with values from 1 to 8. Figures 3(a) and 3(b) show the values of polarization for PMN-0.3PT, as a function of cell number, n, at 300 K, with $\gamma = \delta = 5$ for 71° and 109° uncharged walls, respectively. For the 71° wall, P_1 and P_3 are equal, whereas for the 109°wall P_1 and P_2 are equal. The values of polarization as a function of position are virtually independent of whether the walls are charged or uncharged. However, for the strain distributions there are some differences in peak amplitude between charged and uncharged walls. Those shown in Figs 3(c) and 3(d) are for uncharged 71° and 109° walls with $\gamma = \delta = 5$; the corresponding stress distributions are shown in Figs. 3(e) and 3(f). The summation of stresses over all cells approximates to zero within the accuracy of the calculation.

The simulations confirm that a Néel wall emerges as the stable solution in all cases, with structures as proposed above: i.e. the 71° and 109° wall centers assume orthorhombic and tetragonal symmetries respectively. It is notable that the value of P_3 at the center of the 109° wall is significantly greater than that of P_3 and P_1 in the 71° wall.

The increase in energy density caused by the presence of a domain wall, increases with δ in an almost linear relationship, as shown in Fig. 4(a), with little difference between charged and uncharged walls. The 109° walls represent approximately twice the energy cost of 71° walls for the same values of γ and δ.

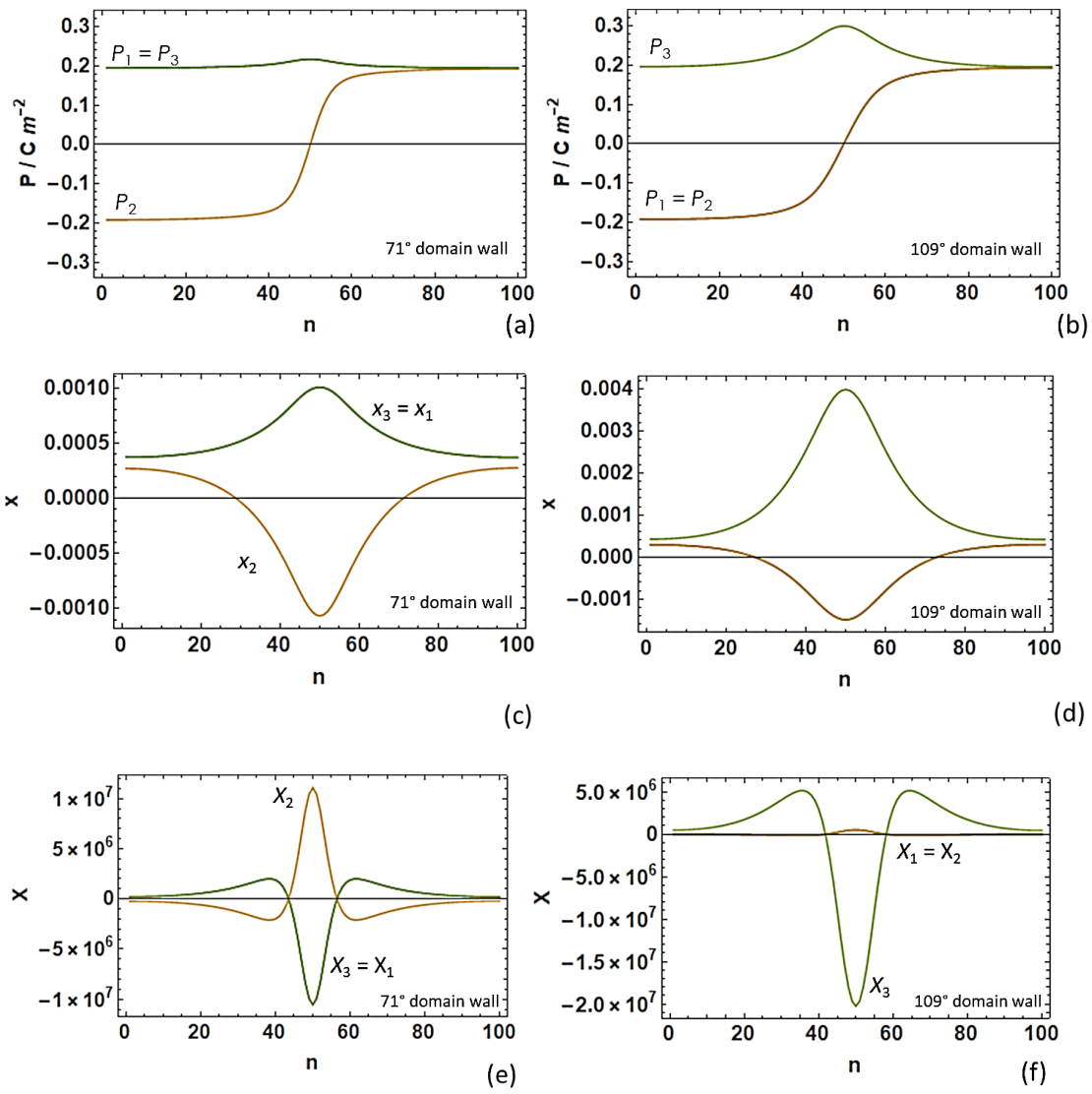

Figure 3. (a) and (b) Polarization, (c) and (d) lattice strain and (d) and (e) stress as a function of position for 71° and 109° domain walls.

Defining the width of the domain wall is not trivial. In fact, $P_3(n) > |P_2(n)|$ for all values of n, implying that the presence of a domain wall imposes monoclinic symmetry throughout the domains, albeit with vanishingly small distortion from the parent rhombohedral symmetry at n = 0 and 100. Hence it is apparent how a material with a rhombohedral ground state, but with a high density of domain walls, may appear to have monoclinic symmetry in diffraction experiments. [7] We define the wall half-width $w_{1/2}$ as the number of cells between the two positions at which P_3 is equal to half the difference between its maximum and minimum values. As shown in Fig. 4(b), the dependence of $w_{1/2}$ on γ is slightly sub-linear, but with surprisingly little variation between the 4 types of wall. Due to the cancellation of units in Eqn. 4, both γ and the cell width are effectively dimensionless; hence $w_{1/2}$ also defines the ratio of domain wall width to domain width.

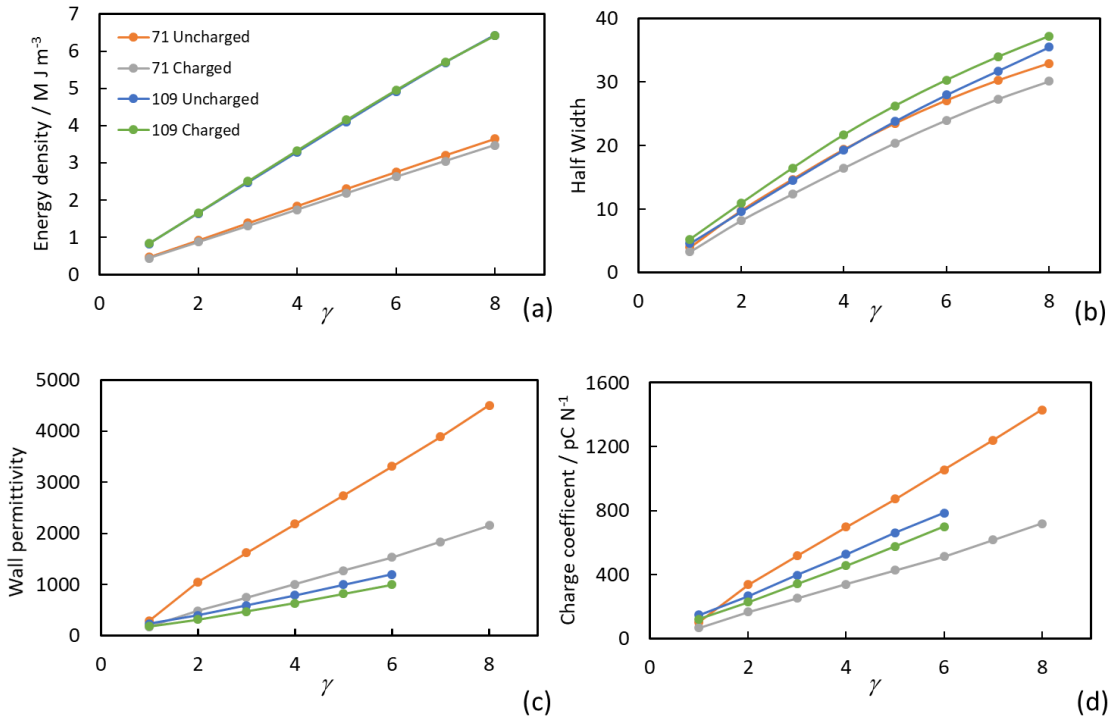

Figure 4. (a) Excess energy density, (b) half-width, (c) permittivity contribution and piezoelectric charge coefficient contribution of domain walls as a function of equal polarization (γ) and strain (δ) coherence length.

3.3 Weak-Field Properties

The contributions of the domain wall to permittivity and piezoelectric charge coefficient averaged across the full range of n, as a function of coherence lengths, γ and δ, are shown in Figs. 4(c) and (d) respectively. All the contributions are positive, and virtually linearly dependent upon γ. The relative permittivity of the uncharged 71° wall exceeds 4500 at γ = 8, whilst that of the 109° walls without strain gradient energies exceeds 1000 for γ = 6. For 109° walls beyond γ = 6, the calculations of permittivity and piezoelectric charge coefficient become unreliable as the width of the walls starts to extend beyond the width of the model. All the above trends are repeated in the piezoelectric charge coefficients (Fig. 4(d)), with the uncharged 71° wall contributing an excess charge coefficient of more than 1400 for γ = 8.

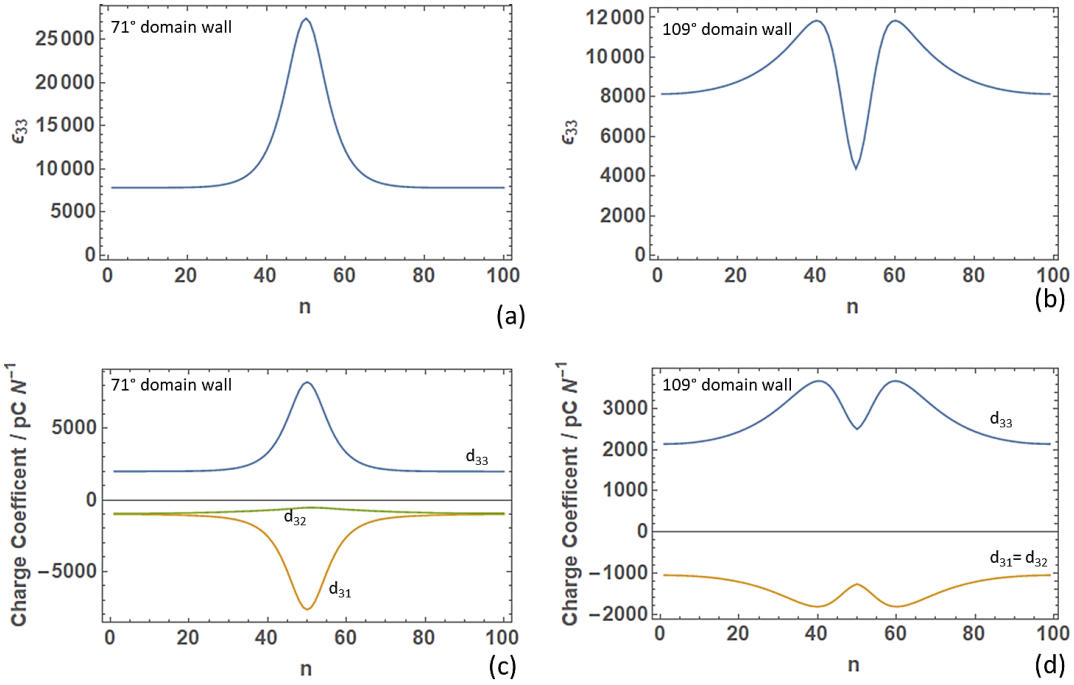

Figure 5. The variation across uncharged domain walls of the permittivity (ε_{33}) for (a) 71° and (b) 109° domain walls and the piezoelectric charge coefficients (d_{33}, d_{31} and d_{32}) for (c) 71° and (d) 109° walls at 300 K for γ = δ = 5.

The variation of the permittivity ε_{33} across 71° and 109° walls at 300 K is shown in Figs. 5(a) and (b) for $\gamma = \delta = 5$. For the 71° wall, ε_{33} passes through a maximum at the orthorhombic wall center, due to the field induced increase in P_3 at the expense of P_1 and P_2, rotating the resultant polarization vector in a *(010)* plane (M_C symmetry). This is an easier path than from *[111]* to *[001]* via M_A, which the bulk material experiences. In contrast, in the 109° wall, ε_{33} passes through a minimum at the tetragonal wall center and exhibits a lower permittivity than the bulk materials. This is consistent with the fact that at the wall center, the polarization is already oriented along *[001]* and therefore no rotation occurs under applied field. However, there are peaks in permittivity in the wall margins, where the symmetry corresponds to M_A and polarization rotation in a *(110)* plane occurs. Hence the overall contribution of the 109° wall to ε_{33} is also positive.

The variation of the charge coefficients across the domain walls (Figs. 5(c) and 5(d)) reflects that of the permittivity. For the 71° wall, whilst d_{33} and $-d_{31}$ pass through maxima at the wall center, d_{32} tends towards zero. However, for the 109° wall, the permittivity and all three charge coefficients are at a minimum at the wall center, with the maximum values occurring in the wall margins. In this case $d_{31} = d_{32}$ throughout. Again, this is consistent with the fact that at the wall center, the polarization is oriented along *[001]* at zero field and therefore no rotation occurs under applied fields. However, the enhanced contributions in the margins are through polarization rotations in the *{110}* planes.

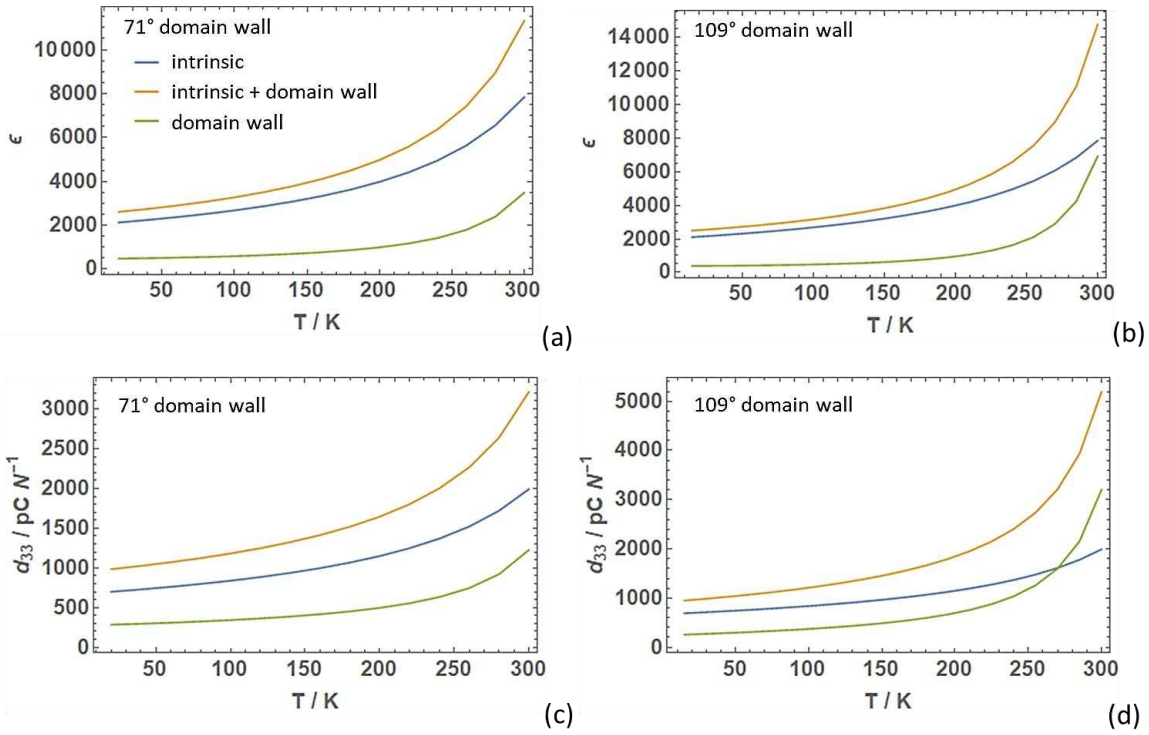

Figure 6. Relative permittivity for uncharged (a) 71° and (b) 109° domain walls and piezoelectric charge coefficient for charged (c) 71° and (d) 109° domain walls; for $\gamma = \delta = 6$.

$\Delta\varepsilon_{33}$ as a function of temperature is shown in Figs. 6(a) and 6(b), for uncharged domain walls with $\delta = 6$. For 71° walls, $\Delta\varepsilon_{33}$ decreases from a value of 4000 at 300K to a minimum of 500 at approximately 0 K. For 109° walls, the permittivity contribution at 300 K is approximately 7000, considerably larger than that for 71° walls, however, it decreases continuously with decreasing temperature to 500 at 0 K.

For a 71° domain wall (Fig. 6(c)), the contribution to the average charge coefficient at 300 K is approximately 1200 pC N^{-1}, decreasing with temperature to 300 pC N^{-1} at 0 K. On the other hand, the contribution of the 109° wall is >3000 pC N^{-1} at 300 K (Fig. 6(d)), 50% larger than the intrinsic value, but decreases continuously with temperature to a value only 30% of the lattice contribution at 0 K.

3.4 High Field Properties

Figure 7 shows how the polarization rotation progresses with increasing field for the case of $\delta = 3$. To recap, at zero field, the domain symmetry is rhombohedral, whilst for

the 71° domain wall, the center is orthorhombic with domain wall margins exhibiting M_B symmetry. For the 109° wall, the center is tetragonal, with M_A margins.

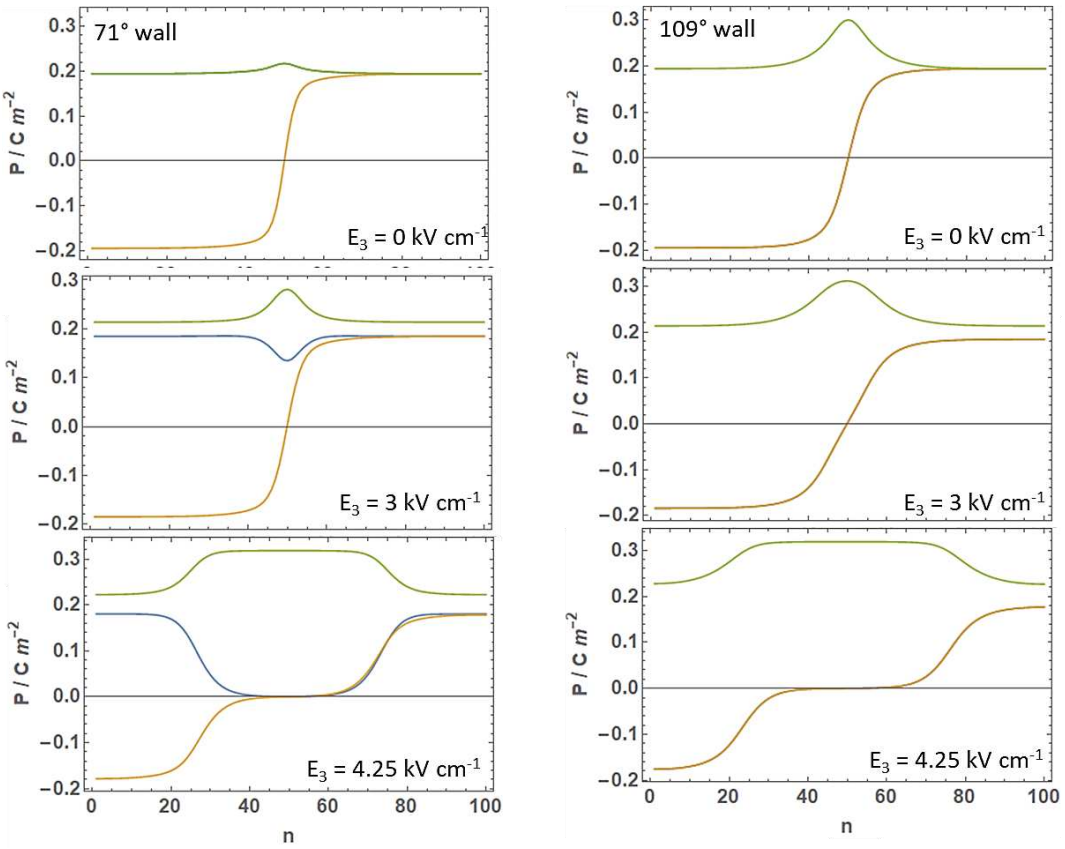

Figure 7. Polarization profile for 71° and 109° domain walls for δ=3 at applied fields of 0, 3 and 4.25 kV cm^{-1}; for higher fields $P_1 = P_2 = 0$ and P_3 > 0.32 C m^{-2} for all values of n.

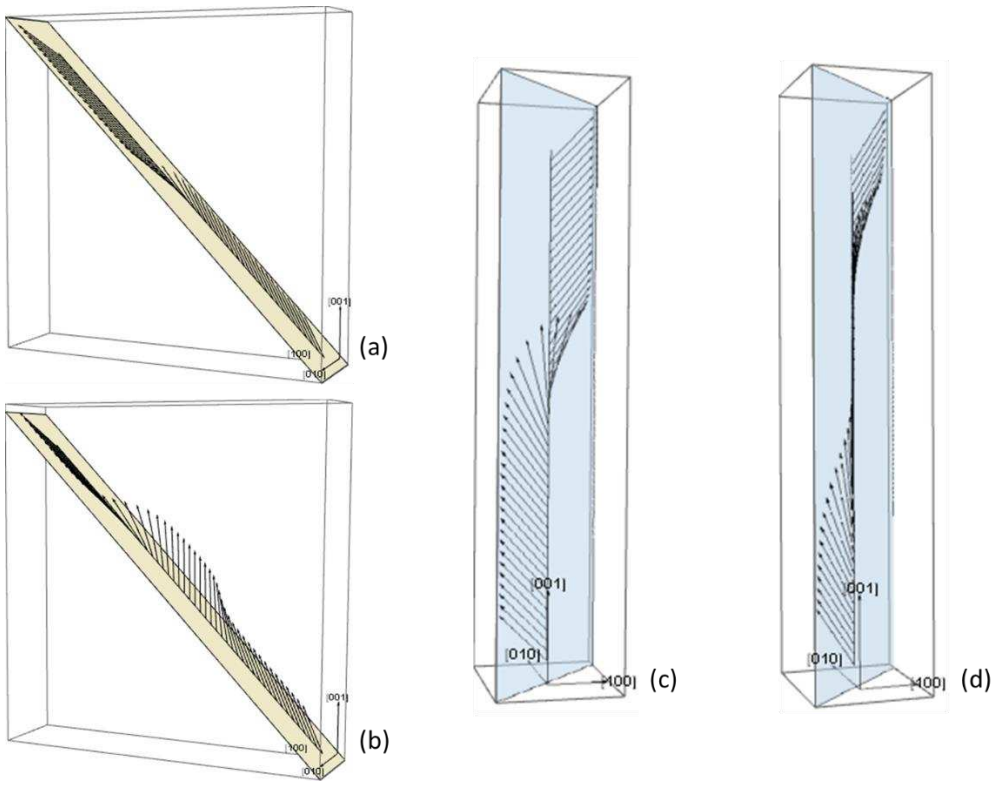

Fig. 8. Polarization directions through (a) an uncharged 71° domain wall at 0 kV cm^{-1} and (b) 4 kV cm^{-1} and through an uncharged 109° wall (c) at 0 kV cm^{-1} and (d) at 4 kV cm^{-1}.

Up to 3 kV cm^{-1}, a similar broadening of both types of domain wall is apparent. For the 71° wall there is divergence between the values of P_2 and P_3 in all cells, whilst at the wall center P_1 = 0 and P_2 is depressed compared to the value in the domain itself. Hence, whilst there is some polarization rotation in the domain, which has assumed M_A symmetry, there is greater rotation in the domain wall, which now exhibits M_C symmetry at the center. As the field is increased the domain wall broadens to cover more than 50% of the domain width at 4.25 kV cm^{-1}. The symmetry over most of the 71° domain wall approximates to M_C. This is emphasized in Fig. 8, showing the direction of polarization in Cartesian coordinates through the domain walls. At zero applied field (Fig. 8(a)), the polarization lies within the *(101)* plane, whilst with a field applied along *[001]*, the polarization within the 71° domain wall rotates out of the *(101)* plane towards the *[001]*, with the angle of rotation being greatest at the center of the wall (Fig. 8(b)).

Above 4.25 kV cm^{-1} the whole crystal switches into the tetragonal state. Overall, the presence of 71° domain walls at sufficiently high density would give the appearance of a crystal that follows a high-field polarization rotation path that starts as M_A but switches to M_C at higher fields before reaching the tetragonal state. Such a path is disallowed by symmetry considerations under the homogeneous 6th order LGD model, but is commensurate with experimental observations. [7]

For the 109° wall, similar broadening is observed as a function of field, however P_1 is equal to P_2 in all cells and the resultant polarization vector remains in the (110) plane throughout the wall at all fields (Figs. 7(c), 7(d) 8(c) and 8(d)). Hence the symmetry is M_A throughout the domain and the wall margins, but with a central region that approximates to tetragonal symmetry that broadens significantly with increasing field. Hence for 109° domain walls the experimentally observed rotation path would be predominantly M_A in symmetry.

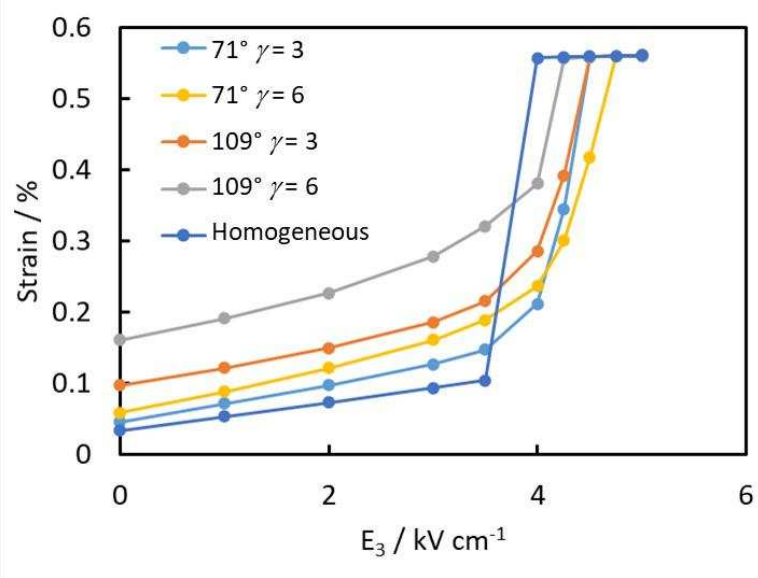

Figure 9. Field induced strain as a function of $\gamma = \delta$ for 71° and 109° domain walls compared with the single domain response.

The average strain across uncharged walls as a function of applied field is shown in Fig. 9 for $\gamma = \delta = 3$ and $\gamma = \delta = 6$, in comparison with the homogenous, domain-free model. The first-order nature of the field-induced rhombohedral-tetragonal transition is

modified by domain wall broadening to a more continuous transformation. The field required to complete the transformation to tetragonal appears to increase with respect to the infinite single domain, however this could be due to convergence issues at higher fields. Nevertheless, despite the presence of domains encouraging polarization rotation and acting as nucleation sites for this process, they do not decrease the transition field. This is to be expected, as a homogeneous tetragonal phase is not stable below the critical phase calculated by the simple Landau-Devonshire model. For both types of wall, the slope below the transition is significantly increased by the presence of the domain walls, confirming their role in enhancing the piezoelectric coefficient. Although the piezoelectric coefficient increases with increasing γ, the induced strain prior to transition is seen to decrease. This is because the centers of the domain walls already possess larger strain components parallel to $[001]$ than the homogenous case. The greater the value of δ, the greater is the width of the domain wall or domain wall density, therefore for the 109° wall there is less volume subject to the full polarization rotation from $[111]$ to $[001]$.

4. Discussion

The Landau-Devonshire model for a single, infinite domain of PMN-0.3PT, using the coefficients of Zhang, [27] shows that at low fields, the piezoelectric properties are dominated by macroscopic polarization rotation via M_A symmetry, with no temperature-activated mechanisms implied. At higher fields the rotation continues but is superseded by a 1st order transition directly into the tetragonal phase. Neither M_B nor M_C symmetries are favored as rotation paths by this model. Under weak fields, at room temperature, the calculations suggest that macroscopic polarization rotation is a valid model. However, both the high-field and low temperature properties are a poor match

to experiment in terms of the low temperature relaxation and the observation of M_C symmetry at high field.

The results from the Landau-Ginzburg domain wall model in *[001]*-poled crystals can explain several of the experimentally observed features. According to the model, the preferred structure for both 71° and 109° domain walls corresponds to the Néel-type, in which the polarization vector rotates in the *[110]* plane through either a *[101]* (71°) or *[001]* (109°) direction, with only small modulations of the resultant magnitude. Hence, at the center of the wall, the structure corresponds to orthorhombic perovskite symmetry for the 71° wall and tetragonal symmetry for the 109° wall. The symmetries in the wall margins correspond to monoclinic M_B and M_A respectively. Hence for certain conditions of composition and values of coherence length the model would suggest average symmetries that are monoclinic and not normally observed in a simple 6th order Landau model.

The model predicts that for *[001]*-poled crystals, on the application of a field parallel to *[001]*, the domain walls can make significant contributions to both the permittivity and piezoelectric charge coefficient, with the magnitudes dependent upon the value of γ. In the case of 71° walls, the augmentation in ε_{33} and d_{ij} is due to a larger field-induced increase in P_3 at the center of the wall than in the domain, corresponding to an augmented rotation of the polarization at the center of the wall away from *[011]* towards *[001]* and accompanied by broadening of the wall. For 109° walls, the augmentation of properties originates in the wall margins rather than the wall center.

For unpoled crystals, for walls with a negative P_3 component, the polarization and piezoelectric contributions are out of phase with those with a positive P_3 component. Assuming equal populations of walls with positive and negative P_3 components, the wall contributions would average to zero, hence the wall-augmented

properties and any accompanying relaxations would not be observed in unpoled crystals. After *[001]*-poling, there is an increase in permittivity commensurate with the removal of the negative-P_3 walls. However, for *[111]* poled crystals, all domain wall contributions including 180° wall translations are removed, resulting in a reduction in permittivity parallel to *[111]*. These arguments are consistent with the experimental data of Shepley [14].

At high field, the symmetry of the 71° walls tends towards M_C with increasing field before the switch to tetragonal, whereas the 109° walls are dominated by M_A symmetry. Given the experimental observation of high field switching from rhombohedral to tetragonal via both M_A and then M_C symmetries, it seems likely that both types of domain are present in poled samples, as observed experimentally by Chang et al. [15]

The experimental data for PMN-PT from Martin et al. [11] shows the low temperature relaxation for PMN-PT is characterized by permittivity step of $\Delta\varepsilon_{33}$ = 2000 to 3000. Assuming 71° walls to be dominant, this range of $\Delta\varepsilon_{33}$ is consistent with a model value of γ = 5 and $w_{1/2}$ of 20.

Assuming domain walls to be responsible for all the augmentation in properties, the relaxation of these properties below 100 K requires explanation in the context of the model. In the case of classical ferroelectrics such as $BaTiO_3$ [19, 20] similar low temperature relaxations have been attributed to the thermal activation of domain wall translation contributions. The most frequently cited mechanism is that thermal activation is required to overcome pinning of the domain walls by defects. It has been argued that dipolar defect pairs formed from oxygen vacancies and cation acceptor impurities, aligned with the local polarization direction, impose an energy barrier sufficient for domain wall translation to freeze out at cryogenic temperatures. By direct

analogy, we propose that domain wall broadening in *[001]*-poled PMN-PT crystals is also temperature activated due to defect states in the wall and the surrounding environment that act to inhibit polarization rotation and wall broadening.

Whilst the model shows that domain wall broadening is a potential mechanism for property enhancement seen in PMN-PT single crystals, there are a number of shortcomings of the model which need to be considered. Firstly, the concept of the Ginzburg approach results in an approximation, which avoids a full treatment according to Maxwell's equations and in the case of the elastic interactions a full mechanics analysis. The way in which head-to-head domains are treated in the Ginzburg model may be judged to be suboptimal. Also, in this specific case, we have employed Landau-Devonshire coefficients derived form a real material, which may already have embedded within them the phenomena we are attempt to model. At worst, this may lead to an overestimate of the property augmentation due to wall broadening, but does not negate the existence of the phenomenon itself. For comparison, we have also applied the model to $BaTiO_3$ at a temperature close to the rhombohedral-orthorhombic phase transition. Although wall broadening is observed, the contribution to the permittivity is actually negative, highlighting the importance of a true MPB to the positive domain wall contributions in PMN-PT. It is also noted that the model treats PMN-PT as chemically homogenous materials, which it clearly is not. We would expect that the chemical heterogeneity may have a controlling influence on the position and paths of domain wall in the crystals. Finally, a further difficulty with the model is that experimental input is required to assign a length scale to the cell size and hence the coherence length. Currently, we do not believe there is sufficient reliability in the estimates of domain wall widths in PMN-PT to provide scaling of the model, but look forward to studies, possibly using transmission electron microscopy, that can provide a quantitative analysis of the

variation of polarization vectors through a domain wall. Whilst all of the above factors may influence the accuracy of the calculations, they do not undermine the basic concept that static walls close to an MPB can increase the permittivity and charge coefficient through broadening via locally enhanced polarization rotation. It remains to be seen whether this this is the dominant extrinsic contribution or whether the PNR model of Li et al. [12, 13] is more important.

The model shares a number of similarities with that proposed by Li [12, 13] In the "PNR model", the cation disorder is responsible for phase heterogeneities, of which the polarization can be aligned with the field more easily than that of the bulk. This process freezes out at low temperature due to the increasing energy difference between the PNRs and the matrix state. In the model proposed here, the domain walls also represent regions of phase heterogeneity which can be aligned more easily with the applied field than can the body of the domain. However, in the latter case, these regions are a natural consequence of the existence of domain walls, which are observed experimentally to exist at high density in these crystals and can be augmented in number by selected poling processes. [15] The high density of domain walls in these crystals is thought to be a consequence of the shallow free energy landscape, with minima representing rhombohedral, tetragonal and orthorhombic states in close proximity in polarization space. The domain wall energies are therefore low, allowing a high density of domain walls to be established. The domain wall density will increase on approaching the MPB as the energy difference between bordering states is reduced, providing an increasing enhancement in properties at the MPB. It has been proposed that the shallow minima are also a consequence of the cation disorder in the system.[28] Hence according to the above findings, both cation disorder and proximity to an MPB are necessary for giant domain wall contributions to piezoelectricity to exist.

5. Conclusions

Given the ubiquitous nature of domain wall contributions to ferroelectric materials and that the domain wall density of PMN-PT single crystals is considered high, it should not be unexpected for the domain walls in this system to make significant contributions to the functional properties. However, until recently, these contributions were ignored as conventional domain wall models are based on domain wall translation. In the case of *[001]*-poled PMN-PT type crystals, the domain walls do not move under subsequent *[001]*-field excursions, however we have shown that the structure of the walls themselves provides easier paths for polarization rotation. Hence it is the material within the domain walls that is responsible for augmentation of weak-field properties over and above that predicted by single domain Landau theory. For higher fields, polarization rotation is augmented, compared to the domain-free state, by broadening of the domain walls leading to further increase in field-induced strain.

It can be argued that the Landau approach is circular, in that the influence of domains is already included in the coefficients. Whilst that may be true, the theory itself is ignorant of the origin of such contributions. This should be borne in mind when considering the quantitative results, where the calculated total of the bulk and domain wall contributions may exceed the experimental values. More importantly, the set of coefficients represent a material that is close to an MPB and the mechanisms of domain wall broadening that result should be considered to be qualitatively correct.

The domain walls are features that break the symmetry of the crystal in such a way as to allow for the observation of M_B and M_C symmetry, which are forbidden under the homogenous 6th power Landau model. This behavior is evident experimentally under high field switching from rhombohedral to tetragonal via the M_C phase and is explained in the model by a superposition of near-M_C walls and M_A domain interiors.

Other heterogeneity-based contributions, such as those described as PNRs by Li et al., [12] may also play a role in enhancing the piezoelectric and dielectric properties and contribute to their low temperature relaxation. However, domain walls are clearly observed experimentally and therefore should be regarded as a likely origin of the anomalous properties. In which case, it is proposed that both cation disorder and proximity to an MPB are necessary for the giant domain wall contributions to piezoelectricity to exist.

6. Acknowledgements

AJB and PMS acknowledge funding by EPSRC [Award EP/R010293/1]. YL acknowledges the support of the China Scholarship Council

7. References

[1] S. E. Park, T. R. Shrout, Ultrahigh strain and piezoelectric behavior in relaxor based ferroelectric single crystals, J. Appl. Phys. , 82, (1997) 1804

[2] S. Zhang, F . Li, High performance ferroelectric relaxor-$PbTiO_3$ single crystals: Status and perspective, J. Appl. Phys. 111 (2012) 031301

[3] Q.F. Zhou, K.H. Lam, H.R. Zheng, W.B. Qiu, K.K. Shung, Piezoelectric single crystal ultrasonic transducers for biomedical applications, Prog. Mat. Sci. 66, (2014) 87

[4] L.M. Ewart, E.A. McLaughlin, H.A. Robinson, J.J. Stace, A. Amin, Mechanical and electromechanical properties of PMNT single crystals for naval sonar transducers, IEEE Trans. Ultrason. Ferro. Freq. Cont. 54 (2007) 2469

[5] S.J. Zhang, S.M. Lee, D.H. Kim, H.Y. Lee, T.R. Shrout, Characterization of Mn-modified $Pb(Mg_{1/3}Nb_{2/3})O_3$-$PbZrO_3$-$PbTiO_3$ single crystals for high power broad bandwidth transducers, Appl. Phys. Lett. 93 (2008) 122908

[6] A.J. Bell, O. Deubzer, Lead-free piezoelectrics — The environmental and regulatory issues MRS Bulletin, 43 (2019) 581

[7] F. Baia, N. Wang, J. Li, D. Viehland, X-ray and neutron diffraction investigations of the structural phase transformation sequence under electric field in 0.7Pb(Mg1⁄3Nb2⁄3)-0.3PbTiO3 crystal, J. Appl. Phys. 96 (2004) 1620

[8] A.A. Bokov, Z.G. Ye, Recent progress in relaxor ferroelectrics with perovskite structure, J. Mat. Sci. 41, (2006) 31

[9] V. Westphal, W. Kleemann, M.D. Glinchuk, Diffuse Phase-Transitions And Random-Field-Induced Domain States of the Relaxor Ferroelectric $Pb(Mg_{1/3}Nb_{2/3})O_3$, Phys. Rev. Lett. 68 (1992) 847

[10] A.F. Devonshire, Theory of Ferroelectrics, Adv. Phys. 3, (1954) 85

[11] F. Martin, H.J.M. ter Brake, L. Lebrun, S. Zhang, T. Shrout, Dielectric and piezoelectric activities in (1−x)Pb($Mg_{1/3}Nb_{2/3}$)O_3−x$PbTiO_3$ single crystals from 5 K to 300 K, J. Appl. Phys. 111 (2012) 104108

[12] F. Li, S.J. Zhang, T.N Yang, Z. Xu, N. Zhang, G. Liu, J. Wang, J. Wang, Z. Cheng, Z-G. Ye, J. Luo, T.R. Shrout, L-Q. Chen, The origin of ultrahigh piezoelectricity in relaxor-ferroelectric solid solution crystals, Nature Comm. 7 (2016) 13807

[13] F. Li, S. Zhang, Z. Xu, L-Q. Chen, The Contributions of Polar Nanoregions to the Dielectric and Piezoelectric Responses in Domain-Engineered Relaxor-$PbTiO_3$ Crystals, Adv. Funct. Mater. 27 (2017) 1700310

[14] P.M. Shepley, L.A. Stoica, Y. Li, G. Burnell, A.J. Bell, Effects of poling and crystallinity on the dielectric properties of Pb($In_{1/2}Nb_{1/2}$)O_3-Pb($Mg_{1/3}Nb_{2/3}$)O_3-$PbTiO_3$ at cryogenic temperatures, Sci. Rep. 9 (2019) 2442; dataset archived at https://doi.org/10.5518/407

[15] W-Y. Chang, C-C. Chung, C. Luo, T. Kim, Y. Yamashita, J.L. Jones, X. Jiang, Dielectric and piezoelectric properties of 0.7 Pb($Mg_{1/3}Nb_{2/3}$)O_3-0.3 $PbTiO_3$ single crystal poled using alternating current, Mater. Res. Lett. 6 (2018) 537

[16] H. Yu, V. Gopalan, J. Sindel, C. A. Randall, Domain switching and electromechanical properties of pulse poled Pb($Zn_{1/3}Nb_{2/3}$)O_3–$PbTiO_3$ crystals, J. Appl. Phys. 89 **(**2001) 561

[17] D.D. Viehland, E.K.H. Salje, Domain boundary-dominated systems: adaptive structures and functional twin boundaries, Adv. Phys. 63 (2014) 267

[18] Y. Zhang, D.Z. Xue, H.J. Wu, X.D. Ding, T. Lookman, X.B. Ren, Adaptive ferroelectric state at morphotropic phase boundary: Coexisting tetragonal and rhombohedral phases, Acta. Mat. 71 (2014) 176

[19] Y. Akishige, T. Nakanishi and N. Mōri Dielectric dispersion in $BaTiO_3$ single crystal at low temperatures, Ferroelectrics, 217, (1998) 217

[20] S. Wada, K. Yako, H. Kakemoto, T. Tsurumi, T. Kiguchi, Enhanced piezoelectric properties of barium titanate single crystals with different engineered-domain sizes, J. Appl. Phys. 98, (2005) 014109

[21] W-F Rao and Y.U. Wang, Domain wall broadening mechanism for domain size effect of enhanced piezoelectricity in crystallographically engineered ferroelectric single crystals, Appl. Phys. Lett. 90 (2007) 041915

[22] V.L. Ginzburg, Some remarks on phase transitions of the 2nd kind and the microscopic theory of ferroelectric materials, Sov. Phys.-Solid State, 2 (1961) 1824

[23] N.A. Petsev, A.K. Tagantsev and N. Setter, Phase transitions and strain-induced ferroelectricity in $SrTiO_3$ epitaxial films, Phys. Rev. B 61 (2000) R825

[24] H.-L. Hu and L.-Q. Chen Three-dimensional computer simulation of ferroelectric domain formation, J. Am. Ceram. Soc. 81 (1998) 492

[25] J. Hlinka and P. Márton, Phenomenological model of a 90° domain wall in $BaTiO_3$-type ferroelectrics, Phys. Rev. B 74 (2006) 104104

[26] B. Völker, P. Márton, C. Elsässer and M. Kamlah, Multiscale modelleing for ferroelectric materials: a transition from the atomic level to phase field modelling, continuum Mech. Thermodyn, 23 (2011) 435

[27] H. Zhang, X. Lu, R. Wang, C. Wang, L. Zheng, Z. Liu, C. Yang, R. Zhang, B. Yang, W. Cao, Phase coexistence and Landau expansion parameters for a $0.70Pb(Mg_{1/3}Nb_{2/3})O_3$-$0.30PbTiO_3$ single crystal, Phys. Rev. B 96 (2017) 054109

[28] F. Li, S.J. Zhang, D. Damjanovic, L.Q. Chen, T.R. Shrout, Ultrahigh piezoelectricity in ferroelectric ceramics by design, Adv. Func. Mat. 28, 2018 1801504

Table 1. Geometrical details of the one-dimensional domain wall models

	71^{o} wall		109^{o} wall	
	uncharged	charged	uncharged	charged
Polarization directions	$[111]/[1\bar{1}1]$	$[111]/[1\bar{1}1]$	$[111]/[\bar{1}\bar{1}1]$	$[111]/[\bar{1}\bar{1}1]$
Common polarization plane	$(10\bar{1})$	$(10\bar{1})$	$(1\bar{1}0)$	$(1\bar{1}0)$
Domain wall plane	(101)	(020)	(002)	(110)
Rotation components	P_2	P_2	P_1 & P_2	P_1 & P_2
Model direction	$[101]$	$[010]$	$[001]$	$[011]$
Coupled strain components	x_{22}	x_{11}, x_{33}, x_{13}	x_{11}, x_{22}, x_{12}	x_{33}

Appendix

The full expansions of the Gibbs (G) and Helmholtz (F) energies employed are shown below using Voigt notation for the elastic terms:

$$\begin{aligned}G = {} & \alpha_{200}(P_1^2 + P_2^2 + P_3^2) \\ & +\alpha_{400}(P_1^4 + P_2^4 + P_3^4)+\alpha_{220}\left(P_1^2(P_2^2 + P_3^2) + P_2^2(P_3^2 + P_1^2) + P_3^3(P_1^2 + P_2^2)\right) \\ & +\alpha_{600}(P_1^6 + P_2^6 + P_3^6) + \alpha_{420}\left(P_1^4(P_2^2 + P_3^2) + P_2^4(P_3^2 + P_1^2) + P_3^4(P_1^2 + P_2^2)\right) + \alpha_{222}P_1^2P_2^2P_3^2 \\ & -E_1P_1 - E_2P_2 - E_3P_3 \end{aligned} \quad \text{(A1)}$$

and

$$\begin{aligned}F = {} & \alpha_{200}(P_1^2 + P_2^2 + P_3^2) \\ & +\alpha_{400}'(P_1^4 + P_2^4 + P_3^4)+\alpha_{220}'\left(P_1^2(P_2^2 + P_3^2) + P_2^2(P_3^2 + P_1^2) + P_3^3(P_1^2 + P_2^2)\right) \\ & +\alpha_{600}(P_1^6 + P_2^6 + P_3^6) + \alpha_{420}\left(P_1^4(P_2^2 + P_3^2) + P_2^4(P_3^2 + P_1^2) + P_3^4(P_1^2 + P_2^2)\right) + \alpha_{222}P_1^2P_2^2P_3^2 \\ & -E_1P_1 - E_2P_2 - E_3P_3 \\ & +\frac{1}{2}c_{11}(x_1^2 + x_2^2 + x_3^2) + c_{12}(x_1x_2 + x_2x_3 + x_3x_1) + 2c_{44}(x_4^2 + x_5^2 + x_6^2) \\ & -q_{11}(x_1P_1^2 + x_2P_2^2 + x_3P_3^2) - q_{12}\left(x_1(P_2^2 + P_3^2) + x_2(P_3^2 + P_1^2) + x_3(P_3^2 + P_1^2)\right) \\ & -2q_{44}(x_4P_2P_3 + x_5P_1P_3 + x_6P_1P_2) \\ & +\delta^2|\alpha_i|\left(\left(\frac{dP_1}{dr}\right)^2 + \left(\frac{dP_1}{dr}\right)^2 + \left(\frac{dP_1}{dr}\right)^2\right) \\ & +\mu^2\left[\frac{1}{2}c_{11}\left(\left(\frac{dx_1}{dr}\right)^2 + \left(\frac{dx_2}{dr}\right)^2 + \left(\frac{dx_2}{dr}\right)^2\right) + 2c_{44}\left(\left(\frac{dx_4}{dr}\right)^2 + \left(\frac{dx_5}{dr}\right)^2 + \left(\frac{dx_6}{dr}\right)^2\right)\right] \end{aligned} \quad \text{(A2)}$$

For the calculation of polarization and strain gradients, r is the vector normal to the domain wall.

The q_{ij} coefficients are related to the more normally quoted Q_{ij} coefficients by

$$\begin{aligned} q_{11} &= c_{11}Q_{11} + 2c_{12}Q_{12} \\ q_{12} &= c_{11}Q_{12} + c_{12}(Q_{11} + Q_{12}) \\ q_{44} &= 2c_{44}Q_{44} \end{aligned} \quad \text{(A3)}$$

As implied in the equations, only the 4th order dielectric stiffness coefficients differ between the Gibbs and Helmholtz energies. The relationship between these two sets can be found at zero stress by setting the energies equal and substituting the strain components with the appropriate $Q_{ij}P_iP_j$ components:

$$\begin{aligned} \alpha_{400}' &= a_{400} + c_{11}\left(\frac{1}{2}Q_{11}^2 + Q_{12}^2\right) + c_{12}Q_{12}(2Q_{11} + Q_{12}) \\ \alpha_{220}' &= \alpha_{220} + c_{11}(2Q_{11}Q_{12} + Q_{12}^2) + c_{12}(Q_{11}^2 + 2Q_{11}Q_{12} + 3Q_{12}^2) + 2c_{44}Q_{44}^2 \end{aligned} \quad \text{(A4)}$$